Editors' Suggestion

Rayleigh-number dependence of the critical vibration frequency in vibrating thermal turbulence

Ze-Lin Huang,[1] Xi-Li Guo,[1] Jian-Zhao Wu,[1,2,*] Bo-Fu Wang,[1] Kai Leong Chong,[1,2] and Quan Zhou[1,†]

[1]*Shanghai Key Laboratory of Mechanics in Energy Engineering, Shanghai Institute of Applied Mathematics and Mechanics, School of Mechanics and Engineering Science, Shanghai University, Shanghai 200072, China*

[2]*Shanghai Institute of Aircraft Mechanics and Control, Zhangwu Road, Shanghai 200092, China*

(Received 27 April 2023; accepted 3 October 2023; published 21 November 2023)

We carry out direct numerical simulations of horizontally or vertically vibrated Rayleigh–Bénard (RB) convection over a wide range of Rayleigh number (Ra) and dimensionless vibration frequency (ω) at fixed Prandtl number $Pr = 4.38$ and dimensionless vibration amplitude $a = 1.52 \times 10^{-3}$. It is shown that the global heat transport (measured by the Nusselt number Nu) is close to the value of standard RB convection in buoyancy-dominant regime at small ω, whereas it is significantly enhanced by horizontal vibration or suppressed by vertical vibration in the vibration-dominant regime at large ω. The division between the two regimes yields a critical vibration frequency ω^*, which indicates the onset of vibration-induced Nu enhancement or Nu reduction. The values of ω^* are obtained based on the fitting between the numerical data and our proposed crossover functions. The dependence of ω^* on Ra is then studied. It is found that the fitted critical frequency exhibits two close scaling relations: $\omega^* \sim Ra^{-0.164}$ in horizontally vibrated RB convection and $\omega^* \sim Ra^{-0.172}$ in vertically vibrated cases. Moreover, based on the competition of the kinetic energy production between buoyancy-dominant and vibration-dominant regimes, a physical model is proposed to predict the scaling behavior between ω^* and Ra, i.e., $\omega^* \sim Ra^{-1/6}$, which agrees well with the measured scaling exponents of our numerical data.

DOI: 10.1103/PhysRevFluids.8.113501

I. INTRODUCTION

Thermally driven convection [1–3], as an effective way to transport heat and mass, is ubiquitous in nature and in many industrial applications. The properties of heat transport, the fundamental features of convective structures and multiscale fluctuations in thermal convection, have been extensively studied in the past few years [1–7]. The control of convective heat transport is also an outstanding topic of the field in past decades with fundamental scientific interests. Additionally, stabilizing or destabilizing convective instability as well as enhancing or suppressing heat transport are crucial in numerous engineering domains. Thus the key question is how to effectively enhance or reduce the dimensionless Nusselt number Nu, which characterizes the global heat flux of the system, at a fixed Rayleigh number Ra that quantifies the intensity of buoyancy effects and describes the convective flow regime [8].

*Corresponding author: jianzhao_wu@shu.edu.cn
†Corresponding author: qzhou@shu.edu.cn

In recent years, various approaches have been investigated for tackling the problem of heat transport control, including the temporal or spatial modulation [9–12], the imposition of magnetic or electric field [13–16], the superimposition of shear, oscillating, or rotating flows [17–20], using wall roughness [21–24], through artificial intelligence method [25,26], etc. Perhaps the most promising approach is the active precise control of heat transport using an implementable method. The most relevant of these active approaches to the control is the introduction of external vibration, which has been proven to be an effective way for achieving significant *Nu* enhancement or *Nu* reduction through creating an "artificial gravity" to dynamically destabilize or stabilize thermal convection [27,28].

It is known that vibration has the ability to drive a supplementary flow when it is applied in a fluid layer subjected to a temperature gradient, which is the so-called thermal vibrational convection (TVC) [28]. Gershuni and Lyubimov [28] synthesized the TVC theory with finite and high vibration frequency, and pointed out that the governing equations of streaming flows can be theoretically deduced using the averaging technique in limit of small amplitude and high frequency. Vibration is usually used to strengthen or diminish thermal convection depending on mutual direction of vibration and temperature gradient [29–31]. Most of the previous works focused on the investigation of the interaction of vibration with thermal convection at low Rayleigh numbers. Demin *et al.* [32] investigated the influence of the angle between the temperature gradient and vibration direction on the onset of instability in an infinite plane layer. Gershuni and Lyubimov [28] found that vibration perpendicular to the temperature gradient has the ability to generate a nonzero mean flow at any amplitude. Farooq and Homsy [33] studied the effect of vibration parallel to the temperature gradient in natural convection, and found the possibility of resonances between the basic flow and vibration-induced higher-order streaming at finite frequency. Cissé *et al.* [34] investigated the Rayleigh-Bénard (RB) convection under vibration of arbitrary direction, and found that high-frequency vibration parallel to the temperature gradient can postpone convective instability; conversely, vibration nonparallel to the temperature gradient generates an average convective flow and influences convective flow. Carbo *et al.* [35] further showed that vertical vibration can postpone the convective instability through the analysis by their proposed computational model. This result is also confirmed by their experiments at low Rayleigh numbers [36]. The influence of vibrational on heat transport has also been addressed at low Rayleigh numbers [37–39]. Forbes *et al.* [37] showed that vibration can enhance the convective heat transport in a rectangular enclosure. Zidi *et al.* [39] showed that vibration aligned to temperature gradient reduces the intensity of the streaming flow and suppresses both the heat and mass transport.

Recently, the investigation of vibrational effects on thermal convection has been extended to the high-*Ra* (i.e., turbulent) regime [40–46]. The suppression of Rayleigh-Taylor turbulence in the zero-gravity condition is achieved after long-time development under the action of the time-periodic vibration aligned to temperature gradient [40]. It is found that vibration parallel to temperature gradient produces a dynamically averaged "antigravity" to stabilize convective flows and significantly suppress heat transport in turbulent RB convection, when the vibration frequency exceeds a critical value [45]. It is also found that vibration perpendicular to the temperature gradient induces the boundary-layer destabilization and achieves a massive enhancement of convective heat-transport rate in both RB convection [41] and vertical convection [42], when the frequency is higher than a critical value. Such massive heat-transport enhancement induced by horizontal vibration is also observed in RB convection over rough surfaces for large vibration frequency [44].

As a typical parameter for the vibrational convective heat transport, the critical frequency ω^* indicates the onset of *Nu*-enhancement or *Nu*-reduction achieved by the action of vibration. Therefore, it is of great interest and fundamental importance to reveal its dependence on the control parameters of the system. In this paper, we chose the paradigm of thermal convection, i.e., turbulent RB convection, and carried out a series of direct numerical simulations of RB convection under the action of horizontal or vertical vibrations over a wide range of Rayleigh number *Ra* and vibration frequency ω. We investigated the effects of vibration on the global heat transport of the system and reveal the dependence of the critical vibration frequency ω^* on *Ra*. The reminder of this

paper is organized as follows. Section II gives a brief description of the governing equations and numerical approach of turbulent RB convection with horizontal or vertical vibration. In Sec. III, we show the transition from buoyancy-dominant regime to vibration-dominant regime, analyze the Ra dependence of ω^*, and then propose a physical model to physically understand the measured ω^*-Ra scaling. Finally, the conclusion is given in Sec. IV.

II. NUMERICAL METHODS

In this section, we give the details of our numerical methods. We consider turbulent RB convection filled with water. All solid walls of the convection cell satisfy the nonslip boundary conditions. Four sidewalls are adiabatic and a uniform temperature is imposed at the top ($T_{\rm cold}$) and bottom ($T_{\rm hot}$) plates. To control the convective heat transport, we apply an external harmonic vibration $A\cos(\Omega t)\boldsymbol{e}_{\rm vib}$ to the system, where A is the vibration amplitude, Ω is the frequency, and $\boldsymbol{e}_{\rm vib}$ is the unit vector in the vibration direction. In the reference frame associated to the imposed vibration, an additional inertial acceleration $A\Omega^2\cos(\Omega t)\boldsymbol{e}_{\rm vib}$ is introduced to the fluid of the RB system. In this work, all physical quantities have been made dimensionless with respect to the cell's height H, the temperature difference between the bottom and top plates $\Delta = T_{\rm hot} - T_{\rm cold}$, the free-fall velocity $\sqrt{\alpha g\Delta H}$, and the free-fall time scale $\sqrt{H/(\alpha g\Delta)}$, where α is the thermal expansion coefficient of water and g is the gravitational acceleration. Hence, the fluid motion in vibrated turbulent RB convection is governed by the dimensionless equations:

$$\nabla\cdot\boldsymbol{u} = 0, \tag{1}$$

$$\partial_t\boldsymbol{u} + (\boldsymbol{u}\cdot\nabla)\boldsymbol{u} = -\nabla p + (Ra/Pr)^{-1/2}\nabla^2\boldsymbol{u} + \theta(\boldsymbol{e}_z - a\omega^2\cos(\omega t)\boldsymbol{e}_{\rm vib}), \tag{2}$$

$$\partial_t\theta + (\boldsymbol{u}\cdot\nabla)\theta = (RaPr)^{-1/2}\nabla^2\theta, \tag{3}$$

where $\boldsymbol{u}$ denotes the velocity field, p the kinematic pressure field, θ the temperature field, and $\boldsymbol{e}_z$ the unit vector in the vertical direction. From Eqs. (1)–(3), it is known that the dynamics of the vibrated RB system is regulated by four nondimensional control parameters: the Rayleigh number Ra, the Prandtl number Pr, the dimensionless vibration amplitude a, the dimensionless vibration frequency ω, i.e.,

$$Ra = \frac{\alpha g\Delta H^3}{\nu\kappa}, \quad Pr = \frac{\nu}{\kappa}, \quad a = \frac{\alpha\Delta A}{H}, \quad \omega = \sqrt{\frac{\Omega^2 H}{\alpha g\Delta}}, \tag{4}$$

where ν and κ are the kinematic viscosity and thermal diffusivity of the working fluid, respectively.

For horizontally vibrated convection, we solve the governing equations, in a rectangular cell of aspect ratio $1:1:0.3$, using the open source spectral element code Nek5000, which has been well validated in numerical simulations of turbulent RB convection [47,48]. The Rayleigh number ranges from $Ra = 10^6$ to $Ra = 10^8$, and the dimensionless vibration frequency ranges from $\omega = 0$ to $\omega = 1700$. For vertically vibrated convection, we solve the governing equations, in a cubic cell, using a second-order finite difference code, which has been validated in our previous works [43,45,49]. The Rayleigh number ranges from $Ra = 10^7$ to $Ra = 10^9$, and the dimensionless vibration frequency ranges from $\omega = 0$ to $\omega = 700$. In both cases, the dimensionless vibration amplitude is set to a constant small value of $a = 1.52\times10^{-3}$ and the Prandtl number is fixed at $Pr = 4.38$, which correspond to a small pulsating displacement $A = 0.1H$ and the working fluid of water with mean temperature 40K, the thermal expansion coefficient $\alpha = 3.8\times10^{-4}$, the temperature difference $\Delta = 40$K. The RB convection containing water under small amplitude vibrations is easily achieved experimentally in practice. Further details of the numerical methods and parameters can be found in our previous works [41,45]. Note that the numerical data have been reported in our previous works [41,45], but here we perform new analysis and focus on the Ra dependence of the critical vibration frequency ω^*, which provides new insights into the problem.

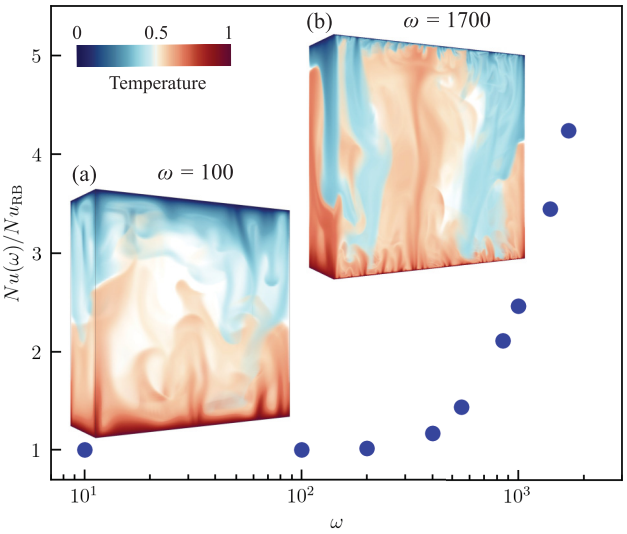

FIG. 1. The normalized Nusselt number $Nu(\omega)/Nu_{\mathrm{RB}}$ as a function of the vibration frequency ω in horizontally vibrated RB convection at fixed Rayleigh number $Ra = 10^8$, where Nu_{RB} is the Nusselt number of classical thermal turbulence without any vibration. The two inserts show the snapshots of instantaneous flow structures visualized by the volume rendering of the temperature field at (a) $\omega = 100$ and (b) $\omega = 1700$.

III. RESULTS

A. Transition from buoyancy-dominant to vibration-dominant regimes

We first examine the vibrational effects on heat transport and flow structures in turbulent RB convection. Figure 1 shows the variation of the normalized Nusselt number $Nu(\omega)/Nu_{\mathrm{RB}}$ as a function of vibration frequency ω at fixed $Ra = 10^8$, where Nu_{RB} is the Nusselt number of classical thermal turbulence without any vibration. The insets (a) and (b) depict the typical snapshots of instantaneous flow structures visualized by the volume rendering of the temperature field at two typical frequencies $\omega = 100$ and $\omega = 1700$, respectively. Here, the Nusselt number is calculated by $Nu = \sqrt{RaPr}\langle u_3\theta\rangle - \partial_{x_3}\langle\theta\rangle$, where u_3 is vertical velocity and $\langle\cdot\rangle$ denotes an average over space and time. When the horizontal vibration is applied, the Nusselt number characterizing the global heat-transfer efficiency of the system initially keeps the value of Nu_{RB} for classical RB convection at small frequency ω, and then is dramatically enhanced when ω exceeds a certain critical frequency. At small frequency (e.g., $\omega = 100$), the vibrational effects are too small to modify the flow pattern, and the overall flow structures are similar to those of classical RB convection as shown in the inset (a) of Fig. 1: the buoyancy effects that yield the convective instability destabilize thermal boundary layers and facilitate the emissions of thermal plumes from the bottom or top plates; those detached plumes move into the bulk regime and then self-organize into the large-scale circulation, which transports heat from the bottom to top plates. At large frequency (e.g., $\omega = 1700$), on the other hand, the vibration effects become so significant. The fast vibration of horizontal plates induces a strong shear to the fluid in the near-wall regions, intensifies the destabilization of thermal boundary layers, triggers massive emissions of thermal plumes, and even breaks the large-scale flow structures, i.e., these detached plumes merge and group together and then form coherent giant plumes as shown in the inset (b) of Fig. 1, which in turn greatly enhances the convective heat transport compared to that in classical RB convection [41].

When the vibration is applied in the vertical direction, the opposite effects of vibration on heat transport are observed as depicted in Fig. 2. It is seen that under the action of vertical vibration,

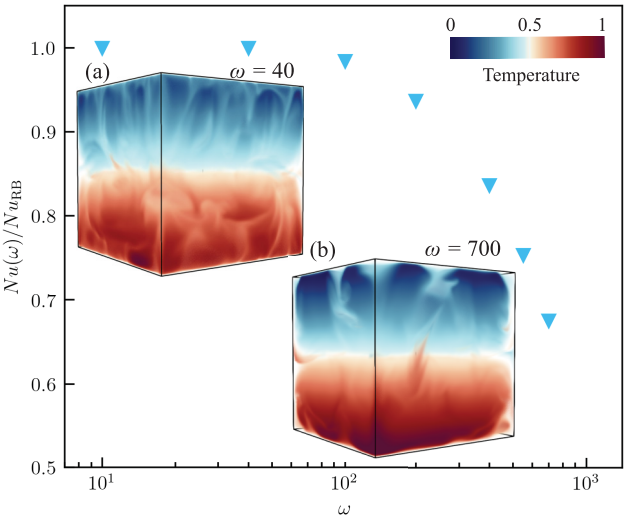

FIG. 2. The normalized Nusselt number $Nu(\omega)/Nu_{\mathrm{RB}}$ as a function of the vibration frequency ω in vertically vibrated RB convection at fixed Rayleigh number $Ra = 3 \times 10^8$. The two inserts show the snapshots of instantaneous flow structures visualized by the volume rendering of the temperature field at (a) $\omega = 40$ and (b) $\omega = 700$.

the ratio of the Nusselt number $Nu(\omega)/Nu_{\mathrm{RB}}$ is initially close to unity, but starts to decrease with increasing ω when exceeding a certain critical frequency. For small frequency (e.g., $\omega = 40$), the vibration effects are too small to balance the gravity and thus the system is still in a state of classical RB turbulence, as shown in the inset (a) of Fig. 2. For large frequency (e.g., $\omega = 700$), vibration-induced dynamical averaging effects (referring to "antigravity" in Ref. [45]) dominate the convective flow, stabilize thermal boundary layers, and suppress the plume ejections as shown in the inset (b) of Fig. 2, which thus reduces the heat-exchange capability of the system.

Briefly, it is found that the vibrational effects on the convective heat transport depend on the relative orientation of vibration to that of temperature gradient. For cases under horizontal vibration, i.e., the vibration direction is perpendicular to that of the temperature gradient (or the gravitation direction), vibration-induced dynamical destabilization results in massive heat-transport enhancement, whereas for cases under vertical vibration, i.e., the vibration direction is parallel to that of temperature gradient, vibration-induced dynamical stabilization leads to significant heat-transport suppression. One sees clearly in Figs. 1 and 2 that for both cases, there exists a critical vibration frequency, denoted as ω^*, below which the buoyancy effect is dominant and vibration nearly does not change the heat-transfer capability, but above which the the vibration effects are significant and vibration can achieve heat-transport enhancement or suppression. The critical vibration frequency ω^*, representing the intensity of the imposed vibration at fixed amplitude a, indicates the transition from the buoyancy-dominant to vibration-dominant regimes in both horizontally and vertically vibrated turbulent RB convection.

B. Scaling between the critical vibration frequency and *Ra*

To reveal the dependence of the critical vibration frequency ω^* on the Rayleigh number, we carried out a series of three-dimensional simulations of both horizontally and vertically vibrated RB turbulence for various *Ra*. Figures 3(a) and 3(b) show the normalized Nusselt number $Nu(\omega)/Nu_{\mathrm{RB}}$ as a function of ω for different *Ra* in horizontally and vertically vibrated RB convection, respectively. Both *Nu* enhancement by horizontal vibration and *Nu* suppression by vertical vibration are observed for all *Ra* studied, suggesting that the effects of vibration on controlling heat transport

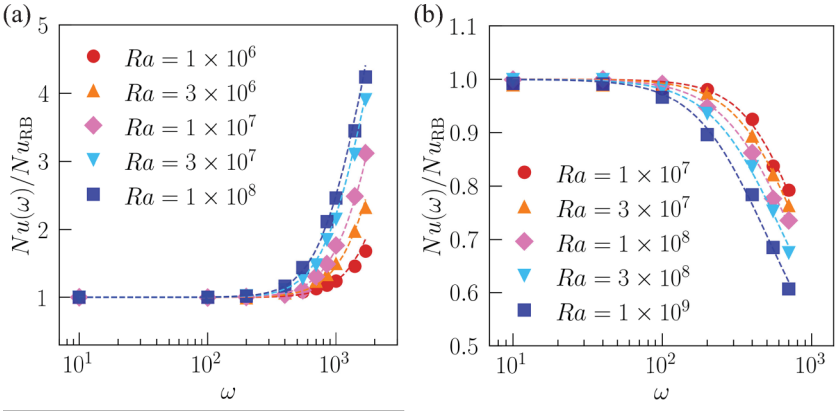

FIG. 3. The normalized Nusselt number $Nu(\omega)/Nu_{\mathrm{RB}}$ as a function of the vibration frequency ω for various Ra in RB convection under (a) horizontal and (b) vertical vibration. In (a) the dashed lines are the best fits of the crossover function $y = \log_{10}[10^{1/4} + (\omega/\omega^*)^{n/4}]^4$ to the respective data. In (b), the dashed lines are the best fits of the crossover function $y = 1/\log_{10}[10 + (\omega/\omega^*)^n]$ to the respective data.

are rather robust in the turbulent regime. In addition, we note that for horizontally vibrated cases, $Nu(\omega)/Nu_{\mathrm{RB}}$ keeps nearly unchanged in the buoyancy-dominant regime (small ω), i.e., $Nu(\omega)/Nu_{\mathrm{RB}} \approx 1$, whereas $Nu(\omega)/Nu_{\mathrm{RB}}$ grows rapidly with increasing ω in the vibration-dominant regime (large ω), exhibiting a roughly linear relation with $\log_{10}(\omega)$ as depicted in Fig. 3(a), i.e., $Nu(\omega)/Nu_{\mathrm{RB}} \approx n\log_{10}(\omega) = \log_{10}(\omega^n)$, where n is an unknown parameter. To crossover from $Nu(\omega)/Nu_{\mathrm{RB}} \approx 1$ in the buoyancy-dominant regime to $Nu(\omega)/Nu_{\mathrm{RB}} \approx \log_{10}(\omega^n)$ in the vibration-dominant regime, we propose an crossover function $Nu(\omega)/Nu_{\mathrm{RB}} = \log_{10}[10^{1/4} + (\omega/\omega^*)^{n/4}]^4$, where ω^* represents the critical vibration frequency. The fitted curves of the crossover function to the respective data as a function of ω are plotted as the dashed lines in Fig. 3(a). Similarly, for cases of vertically vibrated RB convection, we propose a crossover function $Nu(\omega)/Nu_{\mathrm{RB}} = 1/\log_{10}[10 + (\omega/\omega^*)^n]$ to describe the dependence of $Nu(\omega)/Nu_{\mathrm{RB}}$ on ω. The corresponding fitted curves are presented as the dashed lines in Fig. 3(b). It is seen in Figs. 3(a) and 3(b) that all fitted curves agree well with the respective data for both horizontal and vertical vibrations, indicating that these proposed crossover functions can indeed characterize the dependence between the normalized $Nu(\omega)/Nu_{\mathrm{RB}}$ and ω.

To better compare the measured $Nu(\omega)/Nu_{\mathrm{RB}}$ at different Ra, we adopt the fitted values of ω^* to normalize the data and the results are displayed in Figs. 4(a) and 4(b). It is clearly seen that not only the Nu data of horizontal vibration at different Ra collapse well on top of each other, but also the vertical vibration data are nicely coincident together. It is also shown that above the critical frequency ω^*, the Nu enhancement or Nu reduction becomes so significant, and under the normalization of ω^*, the dependence of Nu on ω exhibits some kind of universal properties for all cases studied. This implies that the critical frequency ω^*, signaling the onset of the vibration-dominant regime, is a key parameter for characterizing the vibration-induced enhancement or suppression of the convective heat transport.

Next, we examine the dependence of ω^* on Ra. The fitted ω^* as a function of Ra is shown in Fig. 5. Both ω^*-Ra data sets exhibit a scaling relation and the best power-law fit yields a scaling $\omega^* \sim Ra^\beta$ with a fitted scaling exponent $\beta = -0.164$ for horizontal vibration and $\beta = -0.172$ for vertical vibration. Taking advantage of the scaling of ω^*, the vibration effects on thermal turbulence can be categorized into two regimes: when $\omega < \omega^*$, the classical RB regime is recovered and the vibration effects are too feeble to change the values of Nu; when $\omega > \omega^*$, on the other hand, the vibrational effects dominate the convective flow, and thus the vibration-induced dynamical

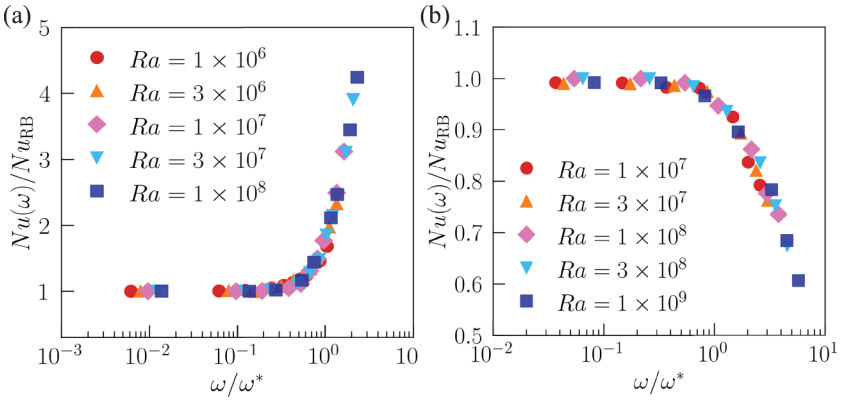

FIG. 4. The normalized Nusselt number $Nu(\omega)/Nu_{\mathrm{RB}}$ as a function of the normalized frequency ω/ω^* for different Ra in turbulent RB convection under (a) horizontal and (b) vertical vibrations. The critical vibration frequency ω^* is obtained through the fitting of the crossover function to the respective data.

destabilization (or stabilization) results in significant Nu enhancement when vibration is applied in the horizontal direction (or Nu reduction when vibration is applied in the vertical direction).

C. Physical model

It is interesting to understand the scaling behaviors of ω^* shown in Figs. 5(a) and 5(b), above which the vibration effects become significant. Note that any physical variable can be divided into a slow part and a fast (pulsational) part, i.e., $u_i = U_i + u_i'$, $\theta = \Theta + \theta'$. Here, the time scale for slow parts (U_i, Θ) is much larger than the vibration period τ_ω, whereas the characteristic time scale of fast parts (u_i', θ') is comparable to τ_ω. The slow parts can be obtained by taking the average of the corresponding physical variables over a vibration period, i.e., $U_i = \langle u_i \rangle_{\tau_\omega}$, $\Theta = \langle \theta \rangle_{\tau_\omega}$ and $P = \langle p \rangle_{\tau_\omega}$. Here, the averaging operator over a vibration period $\langle \phi(t) \rangle_{\tau_\omega}$ can be expressed by

$$\langle \phi(t) \rangle_{\tau_\omega} = \frac{1}{\tau_\omega} \int_t^{t+\tau_\omega} \phi(t')dt', \tag{5}$$

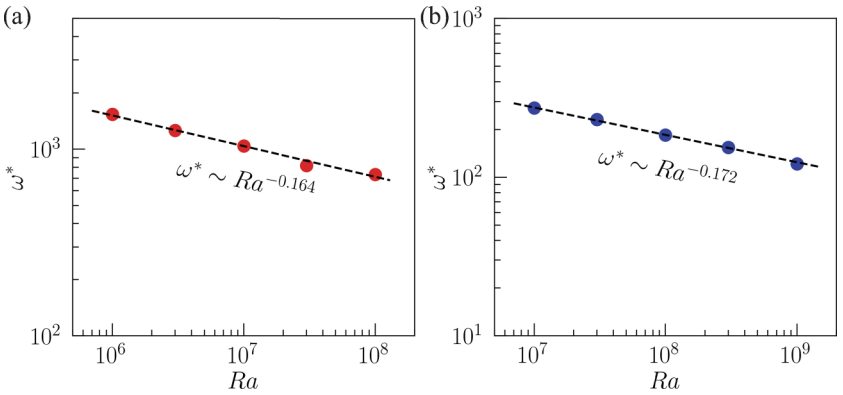

FIG. 5. The fitted critical vibration frequency ω^* as a function of Ra in turbulent RB convection under (a) horizontal and (b) vertical vibrations. The best power-law fit to ω^* yields a scaling $\omega^* \sim Ra^{-0.164}$ in (a) and $\omega^* \sim Ra^{-0.172}$ in (b).

where $\tau_\omega = 2\pi/\omega$ is the vibrational period. Applying this decomposition into the momentum equation, i.e., Eq. (2), allows to write

$$\partial_t U_i + U_j \partial_j U_i = -\partial_i P + \Theta\delta_{i3} - \langle a\omega^2 \cos(\omega t)\theta'\rangle_{\tau_\omega}\delta_{i3} + (\sqrt{Ra/Pr})^{-1}\partial_j\partial_j U_i + \partial_j \tau_{ij}, \tag{6}$$

where $\tau_{ij} = -\langle u_i' u_j'\rangle_{\tau_\omega}$ is the vibrational stress. Multiplying U_i to Eq. (6), we obtain the transport equation of kinetic energy $\mathrm{K} = U_i U_i/2$, namely,

$$\partial_t \mathrm{K} = \mathrm{P} + \partial_k \mathrm{T}_k - \epsilon, \tag{7}$$

where P is the kinetic energy production, T_k is spatial transport flux, and ϵ is the dissipation. In the production term P, it consists of two parts: one is $\mathrm{P}_{\mathrm{gra}}$ driven by the gravitation-induced buoyancy, and the other is $\mathrm{P}_{\mathrm{vib}}$ by the vibrational buoyancy and stress, i.e.,

$$\mathrm{P} = \underbrace{U_3\Theta}_{\mathrm{P}_{\mathrm{gra}}} + \underbrace{(-U_3\langle a\omega^2\cos(\omega t)\theta'\rangle_{\tau_\omega} - \tau_{ij}S_{ij})}_{\mathrm{P}_{\mathrm{vib}}}, \tag{8}$$

where $S_{ij} = (\partial_j U_i + \partial_i U_j)/2$ is the strain tensor.

To quantitatively determine the relative importance of vibrational and gravitational effects in vibrated turbulent RB convection, we introduce their corresponding production terms in Eq. (8) with taking the time- and space-average: the averaged energy production driven by gravitational buoyancy $\overline{\mathrm{P}}_{\mathrm{gra}} = \langle U_3\Theta\rangle$ and the averaged production by the vibration-induced buoyancy and stress $\overline{\mathrm{P}}_{\mathrm{vib}} = \langle -U_3\langle a\omega^2\cos(\omega t)\theta'\rangle_{\tau_\omega} - \tau_{ij}S_{ij}\rangle$. According to the classical averaging theory of TVC [28], one of the solutions for the vibrational parts u_i' and θ' can be found as

$$\boldsymbol{u}_i' = -a\omega\sin(\omega t)N_i, \tag{9a}$$

$$\theta' = -a\cos(\omega t)N_j\partial_j\Theta, \tag{9b}$$

where $N_i = \Theta\delta_{i3} - \partial_i\Phi$ with $\partial_j\partial_j\Phi = \partial_{x_3}\Theta$ and δ_{ij} denoting the Kronecker δ tensor. Substituting Eq. (9) into $\overline{\mathrm{P}}_{\mathrm{vib}}$ yields $\overline{\mathrm{P}}_{\mathrm{vib}} = \langle a^2\omega^2(U_3N_j\partial_j\Theta + N_iN_jS_{ij})/2\rangle$.

We next estimate the magnitudes of $\overline{\mathrm{P}}_{\mathrm{gra}}$ and $\overline{\mathrm{P}}_{\mathrm{vib}}$. From the *Nu* definition, it readily obtains $\overline{\mathrm{P}}_{\mathrm{gra}} \sim \langle U_3\Theta\rangle \sim NuRa^{-1/2}Pr^{-1/2}$. Assuming $|N_i| \sim |\Theta\delta_{i3}| \sim 1$, together with $U_3 \sim ReRa^{-1/2}Pr^{1/2}$, $|\partial_j\Theta| \sim \epsilon_{\mathrm{th}}^{1/2}$, $|S_{ij}| \sim \epsilon_{\mathrm{u}}^{1/2}$, it allows to write $\overline{\mathrm{P}}_{\mathrm{vib}} \sim a^2\omega^2\ (ReRa^{-1/2}Pr^{1/2}\epsilon_{\mathrm{th}}^{1/2} + \epsilon_{\mathrm{u}}^{1/2})$. Here, $|\cdot|$ takes off the magnitude of variables, $\epsilon_u = \langle S_{ij}S_{ij}\rangle$ and $\epsilon_{th} = \langle\partial_j\Theta\partial_j\Theta\rangle$, respectively. According to the relative importance between $\overline{\mathrm{P}}_{\mathrm{gra}}$ and $\overline{\mathrm{P}}_{\mathrm{vib}}$, two regimes can be described as: $\overline{\mathrm{P}}_{\mathrm{vib}} < \overline{\mathrm{P}}_{\mathrm{gra}}$ for the buoyancy-dominant regime and $\overline{\mathrm{P}}_{\mathrm{vib}} > \overline{\mathrm{P}}_{\mathrm{gra}}$ for the vibration-dominant regime. Therefore, at the critical vibration frequency ω^*, one expects a balance between the gravitational and vibrational productions, i.e., $\overline{\mathrm{P}}_{\mathrm{vib}} \approx \overline{\mathrm{P}}_{\mathrm{gra}}$. Combining the exact relations in vibrating RB convection, i.e., $\epsilon_{\mathrm{u}} = Ra^{1/2}Pr^{-1/2}(\overline{\mathrm{P}}_{\mathrm{gra}} + \overline{\mathrm{P}}_{\mathrm{vib}})$, $\epsilon_{\mathrm{th}} - 1 = Ra^{1/2}Pr^{1/2}\overline{\mathrm{P}}_{\mathrm{gra}}$, and $\overline{\mathrm{P}}_{\mathrm{vib}} \approx \overline{\mathrm{P}}_{\mathrm{gra}}$, it readily obtains $\epsilon_{\mathrm{u}} \approx 2Pr^{-1}(\epsilon_{\mathrm{th}} - 1)$ at the critical frequency. Therefore, the balance $\overline{\mathrm{P}}_{\mathrm{vib}} \approx \overline{\mathrm{P}}_{\mathrm{gra}}$ yields $\omega^* \sim a^{-1}Nu^{1/2}Ra^{-1/4}\epsilon_{\mathrm{th}}^{-1/4}\ (ReRa^{-1/2}Pr + 2)^{-1/2}$. As vibration at the critical frequency has a slight influence on the RB system, including the Nusselt number and the Reynolds number, we think that the dependency of *Re* and *Nu* on *Ra* in vibrating RB systems at the critical frequency is very close to that in the standard RB system. Hence, together with $Re \sim Ra^{1/2}$ and $\epsilon_{\mathrm{th}} = Nu \sim Ra^{1/3}$ of classical thermal convection [50], we have

$$\omega^* \sim Ra^{-1/6}, \tag{10}$$

which remarkably agrees well with those of $\omega^* \sim Ra^{-0.164}$ and $\omega^* \sim Ra^{-0.172}$ as shown in Fig. 5 within numerical uncertainty.

IV. CONCLUSIONS

In summary, we considered the issue of controlling heat transport in three-dimensional turbulent RB convection by applying external vibration to the convection cell, and focused on the dependence

of the critical vibration frequency ω^* on Ra, one important control parameter of the RB system. We carried out a series of direct numerical simulations of RB convection under the action of horizontal or vertical vibration over a wide range of the vibration frequency and the Rayleigh number, i.e., $0 \leqslant \omega \leqslant 1700$ and $10^6 \leqslant Ra \leqslant 10^8$ in horizontally vibrated convection, and $0 \leqslant \omega \leqslant 700$ and $10^7 \leqslant Ra \leqslant 10^9$ in vertically vibrated cases. It is found that with increasing ω, the transition from the buoyancy-dominant to vibration-dominant regimes is robustly observed for all Ra studied in both horizontally and vertically vibrated cases. Then, the critical vibration frequency ω^* is proposed to indicate the onset of the vibration-dominant regime, i.e., the onset of Nu enhancement induced by the horizontal vibration or the onset of Nu reduction by the vertical vibration. The values of ω^* are approximately obtained through the fitting of the proposed crossover functions to the corresponding numerical data. It is shown that ω^* and Ra exhibit a close scaling relation, i.e., $\omega^* \sim Ra^{-0.164}$ in horizontally vibrated cases and $\omega^* \sim Ra^{-0.172}$ in vertically vibrated cases. Furthermore, based on the competition of the energy production between the buoyancy-dominant and vibration-dominant regimes, we proposed a physical model and theoretically deduced the scaling relation of the critical vibration frequency, i.e., $\omega^* \sim Ra^{-1/6}$, which agrees well with our numerical results. The present work gives the fundamental basis and practical guideline for the application of the external vibration to control the convective heat transport.

ACKNOWLEDGMENTS

This work was supported by the Natural Science Foundation of China under Grant Nos. 11988102, 92052201, 11825204, 12102246, and 11972220, the Shanghai Science and Technology Program under Project No. 20ZR1419800, the Shanghai Pujiang Program under Project No. 21PJ1404400, and the China Postdoctoral Science Foundation under Grant No. 2020M681259.

[1] G. Ahlers, S. Grossmann, and D. Lohse, Heat transfer and large scale dynamics in turbulent Rayleigh–Bénard convection, Rev. Mod. Phys. **81**, 503 (2009).

[2] D. Lohse and K.-Q. Xia, Small-scale properties of turbulent Rayleigh–Bénard convection, Annu. Rev. Fluid Mech. **42**, 335 (2010).

[3] F. Chillà and J. Schumacher, New perspectives in turbulent Rayleigh–Bénard convection, Eur. Phys. J. E **35**, 58 (2012).

[4] T. Yang, B. Wang, J. Wu, Z. Lu, and Q. Zhou, Horizontal convection in a rectangular enclosure driven by a linear temperature profile, Appl. Math. Mech. Engl. Ed. **42**, 1183 (2021).

[5] X. Zhu and Q. Zhou, Flow structures of turbulent Rayleigh–Bénard convection in annular cells with aspect ratio one and larger, Acta Mech. Sinica **37**, 1291 (2021).

[6] A. Xu, B.-R. Xu, L.-S. Jiang, and H.-D. Xi, Production and transport of vorticity in two-dimensional Rayleigh–Bénard convection cell, Phys. Fluids **34**, 013609 (2022).

[7] Y.-Z. Li, X. Chen, A. Xu, and H.-D. Xi, Counter-flow orbiting of the vortex centre in turbulent thermal convection, J. Fluid Mech. **935**, A19 (2022).

[8] Z. Wang, V. Mathai, and C. Sun, Self-sustained biphasic catalytic particle turbulence, Nat. Commun. **10**, 3333 (2019).

[9] R. Yang, K. L. Chong, Q. Wang, R. Verzicco, O. Shishkina, and D. Lohse, Periodically modulated thermal convection, Phys. Rev. Lett. **125**, 154502 (2020).

[10] Z.-L. Xia, C.-B. Zhao, J.-Z. Wu, B.-F. Wang, and K. L. Chong, Temperature response to periodic modulation in internal heating convection, Phys. Fluids **34**, 125133 (2022).

[11] C.-B. Zhao, Y.-Z. Zhang, B.-F. Wang, J.-Z. Wu, K. L. Chong, and Q. Zhou, Modulation of turbulent Rayleigh-Bénard convection under spatially harmonic heating, Phys. Rev. E **105**, 055107 (2022).

[12] C.-B. Zhao, B.-F. Wang, J.-Z. Wu, K. L. Chong, and Q. Zhou, Suppression of flow reversals via manipulating corner rolls in plane Rayleigh–Bénard convection, J. Fluid Mech. **946**, A44 (2022).

[13] R. Akhmedagaev, O. Zikanov, D. Krasnov, and J. Schumacher, Turbulent Rayleigh–Bénard convection in a strong vertical magnetic field, J. Fluid Mech. **895**, R4 (2020).
[14] J. Wu, P. Traoré, A. T. Pérez, and M. Zhang, Numerical analysis of the subcritical feature of electro-thermo-convection in a plane layer of dielectric liquid, Physica D **311–312**, 45 (2015).
[15] Z. Lu, G. Liu, and B. Wang, Flow structure and heat transfer of electro-thermo-convection in a dielectric liquid layer, Phys. Fluids **31**, 064103 (2019).
[16] J.-Z. Wu, B.-F. Wang, Z.-M. Lu, and Q. Zhou, The heat transfer enhancement by unipolar charge injection in a rectangular Rayleigh–Bénard convection, AIP Adv. **12**, 015212 (2022).
[17] A. Blass, X. Zhu, R. Verzicco, D. Lohse, and R. J. Stevens, Flow organization and heat transfer in turbulent wall sheared thermal convection, J. Fluid Mech. **897**, A22 (2020).
[18] T.-C. Jin, J.-Z. Wu, Y.-Z. Zhang, Y.-L. Liu, and Q. Zhou, Shear-induced modulation on thermal convection over rough plates, J. Fluid Mech. **936**, A28 (2022).
[19] K. Wang, Q. Li, and Y. Dong, Transport of dissolved oxygen at the sediment-water interface in the spanwise oscillating flow, Appl. Math. Mech. Engl. Ed. **42**, 527 (2021).
[20] H. Jiang, D. Wang, S. Liu, and C. Sun, Experimental evidence for the existence of the ultimate regime in rapidly rotating turbulent thermal convection, Phys. Rev. Lett. **129**, 204502 (2022).
[21] D.-L. Dong, B.-F. Wang, Y.-H. Dong, Y.-X. Huang, N. Jiang, Y.-L. Liu, Z.-M. Lu, X. Qiu, Z.-Q. Tang, and Q. Zhou, Influence of spatial arrangements of roughness elements on turbulent Rayleigh–Bénard convection, Phys. Fluids **32**, 045114 (2020).
[22] Y.-Z. Zhang, C. Sun, Y. Bao, and Q. Zhou, How surface roughness reduces heat transport for small roughness heights in turbulent Rayleigh–Bénard convection, J. Fluid Mech. **836**, R2 (2018).
[23] J.-J. Cheng, J.-Z. Wu, Y.-L. Liu, and Z.-M. Lu, Sidewall controlling large-scale flow structure and reversal in turbulent Rayleigh-Bénard convection, J. Turbul. **22**, 380 (2021).
[24] J.-L. Yang, Y.-Z. Zhang, T.-C. Jin, Y.-H. Dong, B.-F. Wang, and Q. Zhou, The Pr-dependence of the critical roughness height in two-dimensional turbulent Rayleigh–Bénard convection, J. Fluid Mech. **911**, A52 (2021).
[25] G. Beintema, A. Corbetta, L. Biferale, and F. Toschi, Controlling Rayleigh–Bénard convection via reinforcement learning, J. Turbul. **21**, 585 (2020).
[26] B. Wang, Q. Wang, Q. Zhou, and Y. Liu, Active control of flow past an elliptic cylinder using an artificial neural network trained by deep reinforcement learning, Appl. Math. Mech. Engl. Ed. **43**, 1921 (2022).
[27] D. Beysens, Vibrations in space as an artificial gravity? Europhys. News **37**, 22 (2006).
[28] G. Z. Gershuni and D. V. Lyubimov, *Thermal Vibrational Convection* (John Wiley & Sons, New York, 1998).
[29] W. Pesch, D. Palaniappan, J. Tao, and F. H. Busse, Convection in heated fluid layers subjected to time-periodic horizontal accelerations, J. Fluid Mech. **596**, 313 (2008).
[30] M. Lappa, Control of convection patterning and intensity in shallow cavities by harmonic vibrations, Microg. Sci. Technol. **28**, 29 (2016).
[31] S. Bouarab, F. Mokhtari, S. Kaddeche, D. Henry, V. Botton, and A. Medelfef, Theoretical and numerical study on high frequency vibrational convection: Influence of the vibration direction on the flow structure, Phys. Fluids **31**, 043605 (2019).
[32] V. Demin, G. Gershuni, and I. Verkholantsev, Mechanical quasi-equilibrium and thermovibrational convective instability in an inclined fluid layer, Int. J. Heat Mass Transfer **39**, 1979 (1996).
[33] A. Farooq and G. Homsy, Streaming flows due to g-jitter-induced natural convection, J. Fluid Mech. **271**, 351 (1994).
[34] I. Cissé, G. Bardan, and A. Mojtabi, Rayleigh Bénard convective instability of a fluid under high-frequency vibration, Int. J. Heat Mass Transfer **47**, 4101 (2004).
[35] R. M. Carbo, R. W. Smith, and M. E. Poese, A computational model for the dynamic stabilization of Rayleigh–Bénard convection in a cubic cavity, J. Acoust. Soc. Am. **135**, 654 (2014).
[36] A. Swaminathan, S. L. Garrett, M. E. Poese, and R. W. Smith, Dynamic stabilization of the Rayleigh–Bénard instability by acceleration modulation, J. Acoust. Soc. Am. **144**, 2334 (2018).
[37] R. E. Forbes, C. T. Carley, and C. J. Bell, Vibration effects on convective heat transfer in enclosures, J. Heat Transfer **92**, 429 (1970).

[38] T. Lyubimova, A. Lizee, G. Gershuni, D. Lyubimov, G. Chen, M. Wadih, and B. Roux, High frequency vibration influence on heat transfer, Microg. **4**, 259 (1994).
[39] E.-h. Zidi, A. Hasseine, and N. Moummi, The effect of vertical vibrations on heat and mass transfers through natural convection in partially porous cavity, Arab. J. Sci. Eng. **43**, 2195 (2018).
[40] G. Boffetta, M. Magnani, and S. Musacchio, Suppression of Rayleigh-Taylor turbulence by time-periodic acceleration, Phys. Rev. E **99**, 033110 (2019).
[41] B.-F. Wang, Q. Zhou, and C. Sun, Vibration-induced boundary-layer destabilization achieves massive heat-transport enhancement, Sci. Adv. **6**, eaaz8239 (2020).
[42] X.-Q. Guo, B.-F. Wang, J.-Z. Wu, K. L. Chong, and Q. Zhou, Turbulent vertical convection under vertical vibration, Phys. Fluids **34**, 055106 (2022).
[43] J.-Z. Wu, Y.-H. Dong, B.-F. Wang, and Q. Zhou, Phase decomposition analysis on oscillatory Rayleigh–Bénard turbulence, Phys. Fluids **33**, 045108 (2021).
[44] J.-Z. Wu, B.-F. Wang, and Q. Zhou, Massive heat transfer enhancement of Rayleigh-Bénard turbulence over rough surfaces and under horizontal vibration, Acta Mech. Sinica **38**, 321319 (2022).
[45] J.-Z. Wu, B.-F. Wang, K. L. Chong, Y.-H. Dong, C. Sun, and Q. Zhou, Vibration-induced 'anti-gravity' tames thermal turbulence at high Rayleigh numbers, J. Fluid Mech. **951**, A13 (2022).
[46] J.-Z. Wu, X.-L. Guo, C.-B. Zhao, B.-F. Wang, K. L. Chong, and Q. Zhou, Unifying constitutive law of vibroconvective turbulence in microgravity, arXiv:2212.08461.
[47] M. Chandra and M. K. Verma, Flow reversals in turbulent convection via vortex reconnections, Phys. Rev. Lett. **110**, 114503 (2013).
[48] A. Pandey, J. D. Scheel, and J. Schumacher, Turbulent superstructures in Rayleigh-Bénard convection, Nat. Commun. **9**, 2118 (2018).
[49] Y.-Z. Zhang, S.-N. Xia, Y.-H. Dong, B.-F. Wang, and Q. Zhou, An efficient parallel algorithm for DNS of buoyancy-driven turbulent flows, J. Hydrodyn. **31**, 1159 (2019).
[50] R. J. Stevens, E. P. van der Poel, S. Grossmann, and D. Lohse, The unifying theory of scaling in thermal convection: The updated prefactors, J. Fluid Mech. **730**, 295 (2013).